

THE OFFICIAL MAGAZINE OF THE OCEANOGRAPHY SOCIETY

# Oceanography

## CITATION

Basu, B. 2018. On a three-dimensional nonlinear model of Pacific equatorial ocean dynamics: Velocities and flow paths. *Oceanography* 31(3):51–58, <https://doi.org/10.5670/oceanog.2018.309>.

## DOI

<https://doi.org/10.5670/oceanog.2018.309>

## COPYRIGHT

This article has been published in *Oceanography*, Volume 31, Number 3, a quarterly journal of The Oceanography Society. Copyright 2018 by The Oceanography Society. All rights reserved.

## USAGE

Permission is granted to copy this article for use in teaching and research. Republication, systematic reproduction, or collective redistribution of any portion of this article by photocopy machine, reposting, or other means is permitted only with the approval of The Oceanography Society. Send all correspondence to: [info@tos.org](mailto:info@tos.org) or The Oceanography Society, 1 Research Court, Suite 450, Rockville, MD 20850, USA.

# On a Three-Dimensional Nonlinear Model of Pacific Equatorial Ocean Dynamics

**VELOCITIES AND FLOW PATHS** By Biswajit Basu

**ABSTRACT.** We investigate the velocity field and the three-dimensional flow paths obtained from a recently developed three-dimensional, nonlinear model that can simulate observed features of the Pacific Equatorial Undercurrent. The sensitivity of the flow field and the paths to the undercurrent are examined. The flow paths or trajectories used in the model were obtained from the exact solution of the velocity field. Nonlinear, three-dimensional features that can be simulated by the model include upwelling/downwelling, cellular flow structures, divergence of flow from the equator and extra-equatorial flows, a subsurface ocean “bridge” in the equatorial direction, and sharp changes in the gradient of the flow path.

## INTRODUCTION

Understanding of the Pacific Equatorial Undercurrent (EUC) is important because contributions to it from various sources profoundly influence the temperature, salinity, and nutrient enrichment of the equatorial thermocline and impact biological productivity, atmospheric carbon exchange, and the El Niño-Southern Oscillation. Known history of the EUC began in the 1950s with its first observations (Cromwell et al., 1954) and measurements (Knauss and King, 1958). McCreary (1981, 1985) provided early models of the current, and among mapping studies, one worthy of mention is the Hawaii-to-Tahiti Shuttle Experiment (Wyrтки and Kilonsky, 1984) conducted as a part of the World Ocean Circulation Experiment. Investigations using global observational models suggest that the Pacific EUC will strengthen in the future (Drenkard and Karnauskas, 2014), and in turn is expected to impact equatorial ocean dynamics.

The EUC is the Pacific cold tongue’s major source of water in the eastern Pacific equatorial region (Wyrтки and Kilonsky, 1984). It is also the primary supplier of the limiting nutrient iron, whose source is sediments from the continental shelf of Papua New Guinea (Rayn et al., 2006). This supply of iron is vital to phytoplankton production that modulates CO<sub>2</sub> fluxes in the equatorial Pacific and controls the export of carbon to the

deep ocean (Feely et al., 2006; Karnauskas and Cohen, 2012; Drenkard and Karnauskas, 2014).

The EUC has also been associated with long-term (decadal) climate variability. Extratropical sea surface temperature (SST) anomalies are transmitted to the tropics by way of intergyre exchange, reappearing along the equator after several years of incorporation into the EUC, and then resurfacing. Existence of a subsurface ocean “bridge” is a possible connection between the warm SST anomaly in the North Pacific during the early 1970s and the subsequent warm SST anomaly along the equator in the 1980s. However, the possible contribution of low-latitude wind stresses to equatorial warming cannot be ignored (Schneider et al., 1999; Hazeleger et al., 2001).

Equatorial ocean dynamics has some striking features. Close to the equator, the meridional component of the Coriolis force is negligible, and it vanishes at the equator. This leads to the breakdown of geostrophy. The flow in this region is essentially driven by winds, the easterly trade winds in the Pacific and Atlantic, and the seasonally reversing monsoonal winds in the Indian Ocean (Talley et al., 2011). Equatorial ocean regions also exhibit pronounced stratification, greater than anywhere else in the ocean (Fedorov and Brown, 2009).

Subjects of undercurrent research include termination, source, divergence, and upwelling (Lukas, 1986; Tsuchiya et al., 1989; Johnson et al., 2001), and undercurrent modeling has employed measurements and observations (McCreary, 1985; Vallis, 2006). The simplest model of the EUC is based on a homogeneous fluid subject to uniform westward stress at the surface. While this local model is unstratified, more realistic models that consider the effects of stratification lead to layered models of undercurrents. Other nonlocal and physical models include a pressure head that is of extra-equatorial origin. Observations indicate that some of the water in the EUC flows from subtropical gyres. A two-layer inertial model of undercurrents can account for equatorial and extra-equatorial dynamics. Initial local theories of undercurrent formation proposed by Cromwell (1953)

were developed further by Stommel (1960), Veronis (1960), and Robinson (1966), and linear non-dissipative models followed (Gill, 1971, 1975; McKee, 1973). Subsequently, linear models were significantly extended to include the effects of continuous stratification (McCreary, 1981), and some nonlinear models were also developed (Charney, 1960; McKee, 1973; Cane, 1979a, 1979b). Inertial theories of Fofonoff and Montgomery (1955) were advanced by Pedlosky (1987), and McCreary and Lu (1994) reconciled the inertial approach with a local perspective that considered the EUC as part of a larger and more complex subtropical current system that has both local and inertial effects. A complete model that captures the integrated dynamics, however, requires numerical computations.

To capture the fine structure of the EUC, the basic variation with depth of its main azimuthal flow can be modeled in the spherical geometry of a rotating Earth (Constantin and Johnson, 2016). However, there are advantages to using the standard  $\beta$ -plane approximation. It permits capture of variations in the meridional direction (in particular, following Earth's curvature) that are not available within the  $f$ -plane approximation framework. (See Constantin and Johnson, 2015, for an overview of ocean dynamics in the equatorial Pacific in the  $f$ -plane setting.) Without further approximations, explicit solutions to the nonlinear governing equations in the equatorial  $\beta$ -plane were recently obtained in the Lagrangian framework (Constantin, 2012, 2014; Constantin and Germain, 2013; Henry, 2013, 2016). These solutions represent realistic flow only for the region near the surface or in the neighborhood of the thermocline. The model does not perform well within the entire vertical extent of the equatorial flow due to the limitations on the permissible underlying currents.

Constantin and Johnson (2017) proposed a model based on the fundamentals of fluid mechanics. This nonlinear, three-dimensional model, herein called the Constantin-Johnson model, is developed following a systematic approach that is mathematically consistent, captures the essential flow properties observed for the Pacific EUC, and avoids oversimplification. For example, the model accounts for the Coriolis effects due to Earth's rotation and retains nontraditional terms arising in the formulation. The model is based on the assumption of slow evolution of a two-layer flow in the equatorial direction, and successfully provides asymptotic solutions.

This article has two goals. One is to study the sensitivity of the EUC model to oceanic flows. The other is to obtain and study Pacific EUC flow paths/trajectories based on the Constantin-Johnson model by identifying the nonlinear three-dimensional nature of the flow, comparing the model with known observations, and exploring the unknowns. Past studies have used trajectory analysis to look at various aspects of the Pacific EUC. A 3.5-layer model was used to study the tropical cells and quantitatively estimate the source of EUC waters (Lu et al., 1998). A relatively coarse resolution Oceanic General Circulation Model

(OGCM) simulation was carried out to quantify local exchanges as the EUC flows from Indonesia to Peru (Blanke and Raynaud, 1997). Other studies examined the mean-time composition of EUC waters (Goodman et al., 2005; Grenier et al., 2011) and variability in pathways of the Pacific EUC (Qin et al., 2015). While increasing computing resources and parameterizing subgrid-scale phenomena have resulted in more realistic simulations, analytically tractable and mathematically consistent models such as the one proposed by Constantin and Johnson, arising out of and satisfying the fluid dynamics equations and principles, are valuable for providing insight into complex nonlinear phenomena. The Constantin-Johnson model has the potential to become an OGCM and to be integrated with other OGCMs for computational efficiency.

This paper focuses on the Constantin-Johnson model and investigates one example from Constantin and Johnson (2017) in detail. The two EUC models considered here, polynomial and quadratic-quartic, both reasonably represent the EUC. The velocity field for the equatorial flow is computed for these two cases, and the results are compared to assess their sensitivity to the model. Three-dimensional flow paths are then derived from the velocity field, and computed trajectories or flow paths are examined to identify features and structures indicative of nonlinear three-dimensional flow.

## RESULTS

Here, we investigate the Constantin-Johnson model. To express the governing equations, we chose a coordinate system that rotates with Earth, with the  $\bar{x}$  axis pointing toward the east, the  $\bar{y}$  axis pointing due north, and the  $\bar{z}$  axis pointing vertically upward (see Figure 1). This description of the coordinate system is, in fact, associated with tangent plane approximation and is also consistent with the  $\beta$ -plane approximation.

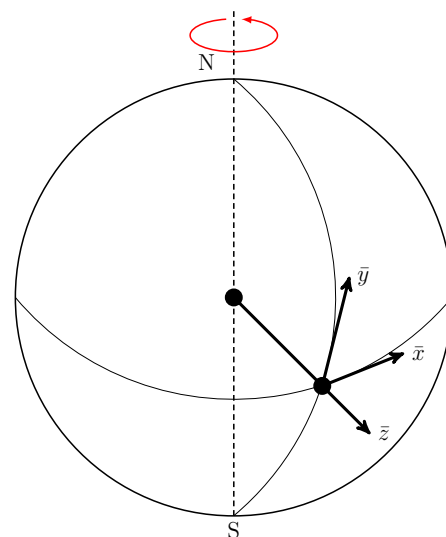


**FIGURE 1.** The rotating frame of reference for Earth with the North Pole, South Pole, the equator, and the rotational axis around the pole indicated.

In this coordinate system, the two set of governing equations (Euler and conservation) may be written as

$$\frac{D\bar{\mathbf{u}}}{D\bar{t}} + 2\bar{\boldsymbol{\Omega}} \times \bar{\mathbf{u}} = -\frac{1}{\bar{\rho}}\bar{\nabla}\bar{p} + \bar{\mathbf{F}}, \quad \bar{\nabla} \cdot \bar{\mathbf{u}} = 0,$$

where  $\bar{\mathbf{u}} = (\bar{u}, \bar{v}, \bar{w})$  is the velocity of the fluid at  $\bar{\mathbf{x}}$  at time  $\bar{t}$ . The operator  $D/D\bar{t}$  is the material derivative, the pressure is  $\bar{p}$ , the (constant) density is  $\bar{\rho}$ , and the body force is represented by  $\bar{\mathbf{F}}$ . The angular velocity vector is  $\bar{\boldsymbol{\Omega}} = \bar{\Omega}(0, \cos \theta, \sin \theta)$ , describing Earth's rotation, with  $|\bar{\boldsymbol{\Omega}}| = \bar{\Omega} \approx 7.29 \times 10^{-5} \text{ rads}^{-1}$  and  $\theta$  the angle of latitude.

### Preliminary Considerations

With a suitable nondimensionalization of the variables, we can write

$$\mathbf{x} = (\bar{x}, \bar{y}, \bar{z}) = (\bar{L}x, \bar{L}y, \bar{h}z),$$

$$\mathbf{u} = (\bar{u}, \bar{v}, \bar{w}) = \bar{U} \left( u, \frac{\bar{L}}{\bar{L}}v, \frac{\bar{h}}{\bar{L}}w \right),$$

We provide some guidelines on the size of some of the parameters. The length is approximately  $13 \times 10^3 \text{ km}$ , the depth to the bottom of the EUC is typically about 200 m, and the width is about 300 km. With these values, and a speed at the surface of  $\bar{U} = 0.5 \text{ m s}^{-1}$ , the nondimensional angular speed of Earth's rotation is  $\omega = \bar{\Omega}\bar{h}/\bar{U} \approx 0.03$ . The choice of scale can be interpreted such that in the flow direction  $0 \leq x \leq 1$ , with  $x = 0$  corresponding to the western end and  $x = 1$  corresponding to the eastern end. The width is restricted to  $-y_0 < y < y_0$  by virtue of  $\beta$ -plane approximation for a suitable finite value of  $y_0$ .

A simplified three-dimensional nonlinear model is derived and a solution is proposed using a suitable approximation of the Coriolis term close to the equator, assuming slow variation of a two-layered flow along the equator and some appropriate simplifying assumptions (Constantin and Johnson, 2017), such as:

1. Small  $r$  (thermocline [pycnocline] is a line of discontinuity in density; above the density is  $\rho_0$  and below the density is  $(1+r)\rho_0$ )
2. Free surface and thermocline sit on planes parallel to tangent plane
3. Constant pressure on the surface along  $y = 0$

Importantly, the formulation considers all of the Coriolis contributions associated with Earth's rotation (see Constantin and Johnson, 2017, for more details on the model). Studies have indicated that ignoring nontraditional components of the Coriolis force influences equatorial ocean dynamics. Constantin and Johnson (2017) provide the solution of the nondimensional velocity field ( $v - w$ ) for the fluid region:

$$\{(x, \zeta) : 0 < x < 1, \zeta_0 < \zeta = z - \frac{1}{2}y^2 < 0\}$$

with  $-y_0 < y < y_0$ . The solution of the velocity field ( $v, w$ ) is dependent on the nature of velocity profile  $u$  or the background undercurrent. The models for background current are mostly based on observations and measurements. For the solution of the equations, we need to specify a profile for the undercurrent

$u$ . Following the proposal by Constantin and Johnson (2017) that mimics observations, we consider two EUC profiles for our investigations: quadratic-quartic and polynomial. The profiles extend down to zero and also have a second zero that replicates the switch from westward to eastward flow near the surface.

The expression for a quadratic-quartic profile can be written as

$$u(x, \zeta) = U(x) - \gamma(x)[\zeta + \lambda(x)]^2 - \delta(x)[\zeta + \lambda(x)]^4$$

for  $0 \geq \zeta \geq -\mu(x)$  and

$$u(x, \zeta) = 0 \text{ for } -\mu(x) > \zeta,$$

while the expression for polynomial profile can be written as

$$u(x, \zeta) = U(x) - \gamma(x)[\zeta + \lambda(x)]^2 - \delta(x)[\zeta + \lambda(x)]^4$$

for  $0 \geq \zeta \geq -\lambda(x)$ ,

$$u(x, \zeta) = U(x) \text{ for } -\lambda(x) \geq \zeta \geq -\mu(x),$$

and

$$u(x, \zeta) = 0 \text{ for } -\mu(x) > \zeta,$$

where

$$\mu = \lambda + \sqrt{-\frac{\gamma}{2\delta} + \sqrt{\frac{U}{\delta} + \frac{\gamma^2}{4\delta^2}}} \quad (1)$$

and  $\lambda(x) = 1 - \Lambda x$ . We assume that

$$U > 0, \gamma > 0, \delta > 0, \mu > \lambda > 0.$$

The uniform maximum azimuthal flow below the surface is located in  $-\lambda(x) > \zeta \geq -\mu(x)$ , and it is assumed that for the model the thermocline is situated somewhere within this maximum azimuthal flow region and not on its boundary.

A complete description of the three-dimensional flow paths requires the solution of the following differential equations simultaneously:

$$dx/dt = u, \quad dy/dt = v, \quad dz/dt = w.$$

Transforming to the  $\zeta$  variable on using  $\zeta = z - \frac{1}{2}y^2$ , we have the following differential equations:

$$dx/dt = u, \quad dy/dt = v, \quad d\zeta/dt = w - v.$$

Numerical integration of the set of differential equations yields three-dimensional streamlines from the three-dimensional velocity field ( $u, v, w$ ). Note that no approximation is made regarding small  $\omega$  in this analysis.

### Example

To carry out the numerical investigations, it is necessary to choose a specific setting with parameters appropriate to a Pacific EUC profile. For this purpose, we consider parameter settings from examples presented in Constantin and Johnson (2017). The value of  $\omega$  is taken as 0.03 for numerical computations in this paper.

We use the parameters considered in Example 3 in Constantin and Johnson (2017). A linear function is used for  $\gamma_0$  given by

$$\gamma_0 = A + Bx,$$

with  $A = 0.03$  and  $B = 2.4$ , approximating  $\gamma$  in Equation 1. We also set  $\hat{U}_0 = 2$  as an approximation of  $U$ , and  $V_0 = 1$  leading to  $c_0 = \hat{U}_0 + V_0 = 3$ . The value of  $\Lambda$  is taken as 0.18. The function  $\delta$  in Equation 1 is approximated by  $\delta_0$ , which is given by

$$\delta_0 = c_0/\lambda^4(x) - \gamma_0(x)/\lambda^2(x).$$

In a three-dimensional plot, Figure 2 shows the horizontal velocity  $v$  and vertical velocity  $w$  in the  $(\zeta - y)$  plane for the quadratic-quartic profile of the EUC for a point on the equator corresponding to  $x = 0.0$  (i.e., at the western end). The variations of the velocity magnitude are plotted vertically as a function of depth function  $\zeta$  and tangential distance due north from the equator  $y$ , at  $x = 0.0$ . As expected, the velocity field exhibits complex structures (see Constantin and Johnson, 2017). The horizontal velocity  $v$  changes sign from positive to negative near the surface, and then assumes a large positive value at an intermediate depth, followed again by a negative value prior to approaching zero deeper down. This fluctuating pattern, clearly evident in Figure 2a, is more pronounced away from the equator. Along the equatorial direction, there is relatively little variation in horizontal velocity. Figure 2b also shows the transformation of negative values of vertical velocity  $w$  near the surface to positive at intermediate depth, subsequently leading to negative values at greater depth. Local troughs and peaks in the vertical

velocity profile increase away from the equator. Along the equatorial direction, the vertical velocity values take on a convex shape, with a maximum positive value at an intermediate depth and negative values both near the surface and deep down. These observations indicate the existence of cellular structures in the oceanic flow (Constantin and Johnson, 2017). To investigate the strength of the flow in the  $(\zeta - y)$  domain, we plot the in-plane velocity amplitude maps ( $u_{in-amp} = \sqrt{v^2 + w^2}$ ) on the  $(\zeta - y)$  plane. Figure 3 portrays two clear regions of strong flow that are located away from the equator at intermediate depth.

To compare the results displayed in Figures 2 and 3 to the case where we consider the polynomial EUC profile, and to examine the sensitivity of the results to two different but reasonable representations of EUC, similar results are plotted in Figures 4 and 5 for the polynomial EUC profile. Figures 4 and 5 demonstrate that the type of EUC profile used affects the results. Figure 4 shows the horizontal velocity  $v$  and vertical velocity  $w$  for the polynomial profile of the EUC in a three-dimensional plot, as in Figure 2, for a point on the equator corresponding to  $x = 0.0$  (i.e., at the western end). It is observed from Figure 4a that variation of the horizontal velocity  $v$  is less compared to that seen in Figure 2a, though the broad nature is somewhat similar. Further, it is observed from Figure 4a that the horizontal velocities are predominantly negative. Again, as in Figure 2a, we

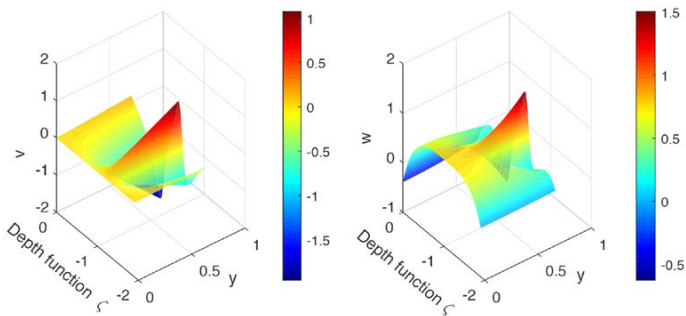


FIGURE 2. (a) Horizontal velocity  $v$ , and (b) vertical velocity  $w$  for a quadratic-quartic profile of the Equatorial Undercurrent (EUC) at  $x = 0.0$ .

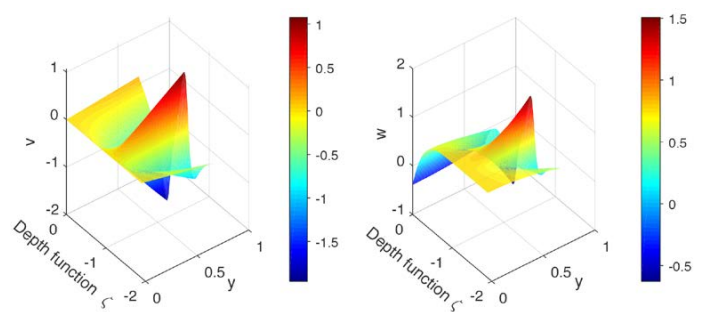


FIGURE 4. (a) Horizontal velocity  $v$ , and (b) vertical velocity  $w$  for a polynomial profile of the EUC at  $x = 0.0$ .

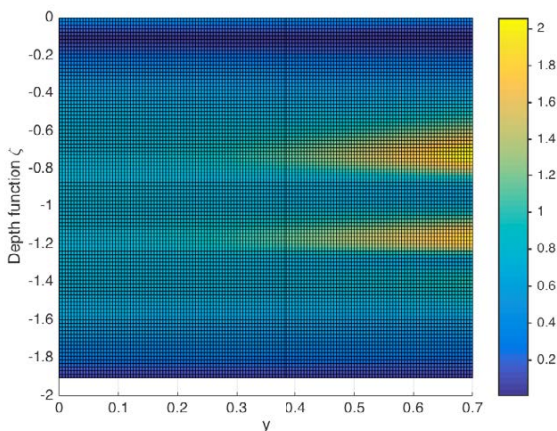


FIGURE 3. In-plane velocity amplitude  $u_{in-amp}$  map for a quadratic-quartic profile of the EUC for  $x = 0.0$ .

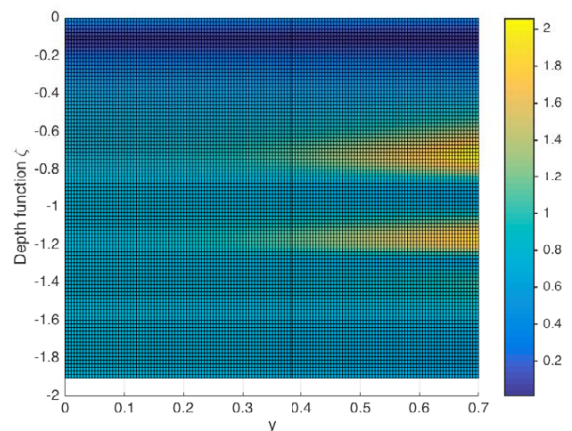


FIGURE 5. In-plane velocity amplitude  $u_{in-amp}$  map for a polynomial profile of the EUC for  $x = 0.0$ .

infer that fluctuations in horizontal velocities along the equator are marginal, as seen in Figure 4a. We also observe from Figure 4b that the vertical velocities are similar in nature to those in Figure 2b, with the exception that the vertical velocities at greater depth in Figure 4b tend to have negative values of higher magnitude. Not much difference is observed in the results between Figures 3 and 5, as both display two strong regions of flow away from the equator at intermediate depth.

Exercises leading to similar types of results as those in Figures 2–5 are produced in Figures 6–9. The results in Figures 6–9 correspond to a point along the equator at  $x = 0.25$ . Broad conclusions from Figures 6–9 derived from the analysis remain unchanged with respect to what was inferred from Figures 2–5, though there are some minor differences. For example, the vertical velocities for the case of a polynomial profile of the EUC attain positive values deep down (around  $\zeta \approx -1.7$  to  $-1.8$ ; see Figure 8) in contrast to negative values for the case of a quadratic-quartic profile of the EUC (see Figure 6).

Next, we use the velocity field to compute the flow path or the trajectories. Because the EUC profile has some impact locally on the velocity (though the broad features of the velocity field are unchanged), we decide to use both EUC profiles once again. We consider the quadratic-quartic profile of the EUC first. The results for the three-dimensional flow paths are plotted in

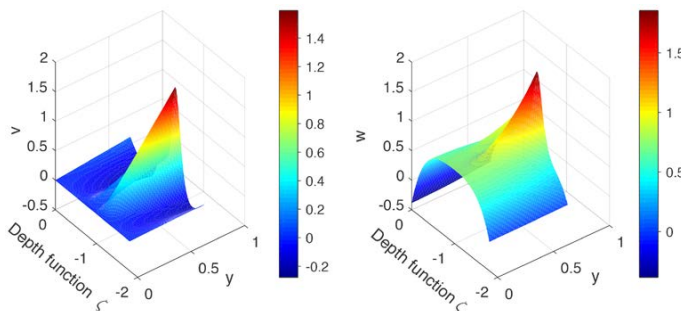


FIGURE 6. (a) Horizontal velocity  $v$ , and (b) vertical velocity  $w$  for a quadratic-quartic profile of the EUC at  $x = 0.25$ .

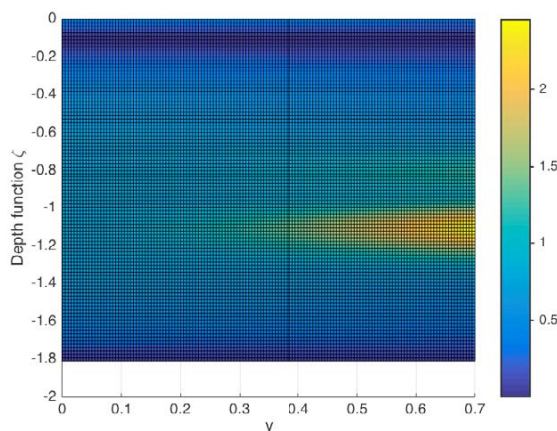


FIGURE 7. In-plane velocity amplitude  $u_{in-amp}$  map for a quadratic-quartic profile of the EUC for  $x = 0.25$ .

Figures 10–12 using the Eulerian velocities in three dimensions obtained previously and performing time integration. We strategically chose nine different initial points at the western end of the equator (i.e.,  $x = 0.0$ ). These nine points represent three groups. The first group chosen is representative of the flow originating near the surface, hence  $\zeta = -0.1$  (i.e., at a depth of 20 m). The second, representing flows originating at intermediate depth, corresponds to  $\zeta = -0.6$  (i.e., at a depth of 120 m). The third group at  $\zeta = -1.2$  (i.e., at a depth of 240 m) initiates flow at greater depth. For each of the groups, the  $y$  positions of the initial points are chosen to be 0.0, 0.3, and 0.6 (i.e., at the equator, approximately 45 km away from the equator, and approximately 90 km away from the equator, respectively).

Figure 10 is a plot of the three-dimensional flow paths from the three initial locations close to the surface ( $\zeta = -0.1$ ) on the  $(\zeta - y)$  plane, corresponding to  $y = 0.0, 0.3,$  and  $0.6$ , respectively. The figure clearly shows the complex three-dimensional nonlinear nature of the paths. Following an initial downward descent, there is a sudden ascent, which is subsequently followed by a sudden sharp drop. This happens around  $x = 0.3$  for all the trajectories. The final phases of the trajectories are monotonically descending in nature, with a gentler slope. The trajectories provide evidence of downwelling, in which waters originating at the western end of the EUC move to the eastern end in a downward-sloping

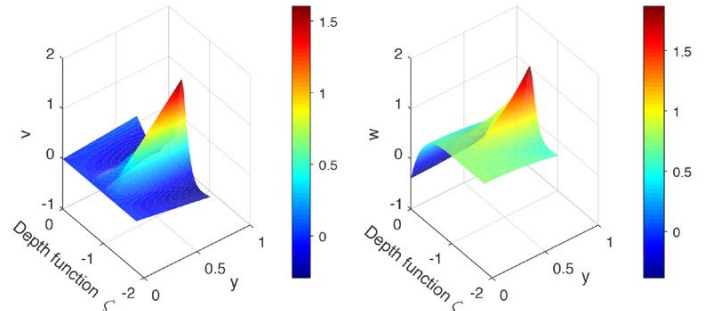


FIGURE 8. (a) Horizontal velocity  $v$ , and (b) vertical velocity  $w$  for a polynomial profile of the EUC at  $x = 0.25$ .

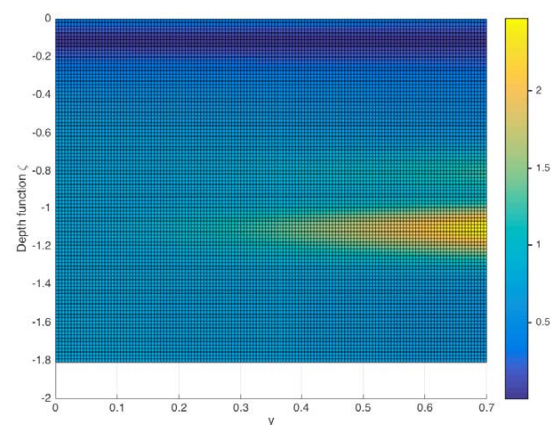


FIGURE 9. In-plane velocity amplitude  $u_{in-amp}$  map for a polynomial profile of the EUC for  $x = 0.25$ .

direction. The paths initiated away from the equator also show some (though marginal) amount of flow toward the equator—demonstrating real three-dimensional structures and confirming that the flow is forced toward the equatorial region.

The three flow paths originating from the  $(\zeta - y)$  plane shown in Figure 11, corresponding to an intermediate depth of  $\zeta = -0.6$ , portray the existence of a subsurface ocean “bridge” in the west-to-east direction. This concept (Zhang et al., 1998) has been used to explain the relationship between the North Pacific and the equator in terms of SST anomaly. In Figure 11, the source water from the western end of the Pacific travels downward before resurfacing at the eastern end. The trajectories in this figure have the tendency to move outward from the equator.

The extra-equatorial flow patterns produced in Figure 11 are amplified in Figure 12, where the originating points of the flow paths at the western end of the equator are located at a relatively

greater depth of  $\zeta = -1.2$  and correspond to  $y = 0.0, 0.3,$  and  $0.6$ . The presence of an extra-equatorial poleward flow path is evident. In fact, originating points farther from the equator show a greater amount of flow divergence from the equator. In addition, we find flows that originate deep down (240 m) at the western boundary of the equator move upward as they move toward the eastern boundary.

Figures 13–15 show results similar to those in Figures 10–12, but for the case of the polynomial EUC profile. The qualitative results in these figures are close to the results observed in Figures 10–12. This is not unexpected as the velocity fields for the two cases of EUC profiles have similar broad natures though they differ in some details. This is translated in the results for flow paths. Hence, the trajectories in Figures 13–15 are similar to the trajectories in Figures 9–12, though there may be some variation in numerical details.

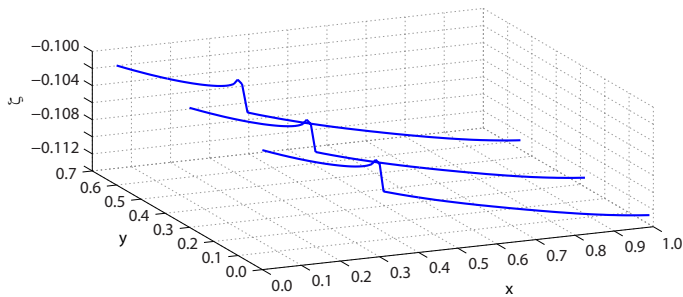


FIGURE 10. Three-dimensional flow paths for a quadratic-quartic EUC profile with paths initiating from points near the surface.

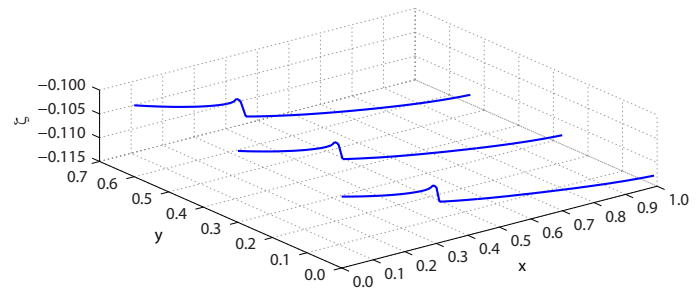


FIGURE 13. Three-dimensional flow paths for a polynomial EUC profile with paths initiating from points near the surface.

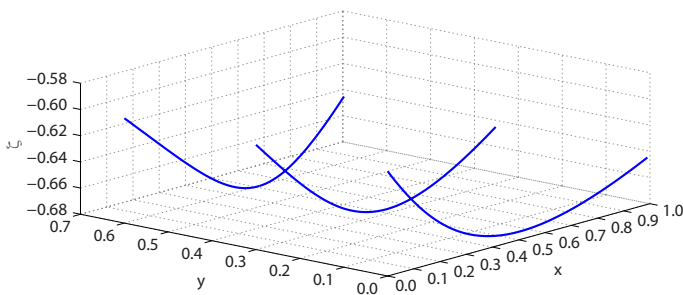


FIGURE 11. Three-dimensional flow paths for a quadratic-quartic EUC profile with paths initiating from points at intermediate depths.

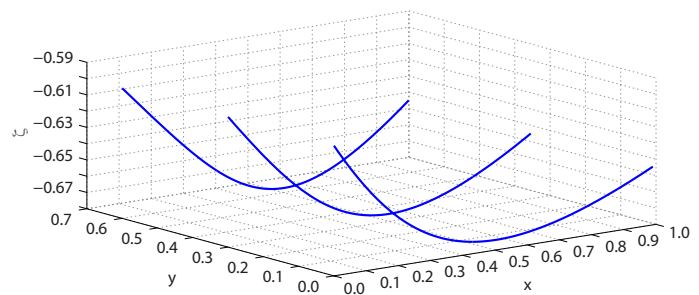


FIGURE 14. Three-dimensional flow paths for a polynomial EUC profile with paths initiating from points at intermediate depths.

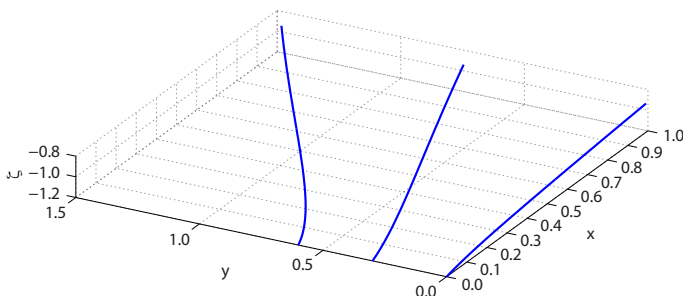


FIGURE 12. Three-dimensional flow paths for a quadratic-quartic EUC profile with paths initiating from points at deeper locations.

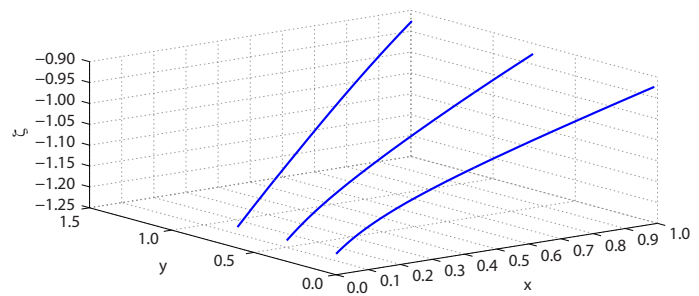


FIGURE 15. Three-dimensional flow paths for a polynomial EUC profile with paths initiating from points at deeper locations.

## CONCLUSION

The investigation carried out in this paper and analyses of the velocity field and flow paths have resulted in a number of observations and findings. Strong flow-field regions exist away from the equator at intermediate depths. Variations of the velocity amplitudes with depth or along the meridional direction are more pronounced away from the equator. Results are similar for the two models of the EUC considered—though the details of the velocity profiles are model sensitive, their broad natures are unaffected by the EUC model used. For example, in the numerical investigation, the vertical velocity attains higher negative values at greater depth for the polynomial profile of the EUC, in contrast to the corresponding velocities obtained for the quadratic-quartic model. Analyses of the flow paths show sharp changes in their gradients. Another remarkable feature observed in this study is the presence of a subsea ocean bridge in the west-to-east direction. Extra-equatorial trajectories, forcing both toward the equator and poleward, have also been observed. In particular, poleward extra-equatorial flow paths originating from a deeper initial source at the western end of the equator are spectacular. All features of the flow path strongly reinforce the three-dimensional nonlinear nature of the flow, and demonstrate that the Constantin-Johnson model is capable of modeling these features, some of which are known from observations and some still possibly unknown. From this study we conclude that the Constantin-Johnson model for Pacific equatorial ocean dynamics shows promise, and with some further development, is a potential candidate to become an Oceanic General Circulation Model. 

## REFERENCES

- Blanke, B., and S. Raynaud. 1997. Kinematics of the Pacific equatorial undercurrent: An Eulerian and Lagrangian approach from GCM results. *Journal of Physical Oceanography* 27:1,038–1,053, [https://doi.org/10.1175/1520-0485\(1997\)027<1038:KOTPEU>2.0.CO;2](https://doi.org/10.1175/1520-0485(1997)027<1038:KOTPEU>2.0.CO;2).
- Cane, M.A. 1979a. The response of an equatorial ocean to simple wind stress patterns: Part I. Model formulation and analytical results. *Journal of Marine Research* 37:232–252.
- Cane, M.A. 1979b. The response of an equatorial ocean to simple wind stress patterns: Part II. Numerical results. *Journal of Marine Research* 6:355–398.
- Charney, J.G. 1960. Non-linear theory of a wind-driven homogeneous layer near the equator. *Deep Sea Research* 6:303–310, [https://doi.org/10.1016/0146-6313\(59\)90089-9](https://doi.org/10.1016/0146-6313(59)90089-9).
- Constantin, A. 2012. An exact solution for equatorially trapped waves. *Journal of Geophysical Research* 117, C05029, <https://doi.org/10.1029/2012JC007879>.
- Constantin, A. 2014. Some nonlinear, equatorially trapped, nonhydrostatic internal geophysical waves. *Journal of Physical Oceanography* 44:781–789, <https://doi.org/10.1175/JPO-D-13-0174.1>.
- Constantin, A., and P. Germain. 2013. Instability of some equatorially trapped waves. *Journal of Geophysical Research* 118:2,802–2,810, <https://doi.org/10.1002/jgrc.20219>.
- Constantin, A., and R.S. Johnson. 2015. The dynamics of waves interacting with the Equatorial Undercurrent. *Geophysical & Astrophysical Fluid Dynamics* 109:311–358, <https://doi.org/10.1080/03091929.2015.1066785>.
- Constantin, A., and R.S. Johnson. 2016. An exact, steady, purely azimuthal equatorial flow with a free surface. *Journal of Physical Oceanography* 46:1,935–1,945, <https://doi.org/10.1175/JPO-D-15-0205.1>.
- Constantin, A., and R.S. Johnson 2017. A nonlinear, three-dimensional model for ocean flows, motivated by some observations of the Pacific equatorial undercurrent and thermocline. *Physics of Fluids* 29, 056604, <https://doi.org/10.1063/1.4984001>.
- Cromwell, T. 1953. Circulation in a meridional plane in the central equatorial Pacific. *Journal of Marine Research* 12:96–213.
- Cromwell, T., R.B. Montgomery, and E.D. Stroup. 1954. Equatorial undercurrent in Pacific Ocean revealed by new methods. *Science* 119:648–649, <https://doi.org/10.1126/science.119.3097.648>.
- Drenkard, E.J., and K.B. Karnauskas. 2014. Strengthening of Pacific Equatorial Undercurrent in the SODA reanalysis: Mechanics, ocean dynamics, and implications. *Journal of the American Meteorological Society* 27:2,405–2,415, <https://doi.org/10.1175/JCLI-D-13-00359.1>.
- Fedorov, A.V., and J.N. Brown. 2009. Equatorial waves. Pp. 3,679–3,695 in *Encyclopedia of Ocean Sciences*. J. Steele, ed., Academic Press, San Diego.
- Feely, R.A., T. Takahashi, R. Wanninkhof, M.J. McPhaden, C.E. Cosca, S.C. Sutherland, and M.-E. Carr. 2006. Decadal variability of the air-sea CO<sub>2</sub> fluxes in the equatorial Pacific Ocean. *Journal of Geophysical Research* 111, C08S90, <https://doi.org/10.1029/2005JC003129>.
- Fofonoff, N.P., and R.B. Montgomery. 1955. The equatorial undercurrent in the light of the vorticity equation. *Tellus* 7:518–521, <https://doi.org/10.3402/tellusa.v7i4.8910>.
- Gill, A.E. 1971. The equatorial current in a homogeneous ocean. *Deep Sea Research and Oceanographic Abstracts* 18:421–431, [https://doi.org/10.1016/0011-7471\(71\)90103-3](https://doi.org/10.1016/0011-7471(71)90103-3).
- Gill, A.E. 1975. Models of equatorial currents. Pp. 181–203 in *Proceedings of Numerical Models of Ocean Circulation*.
- Goodman, P.J., W. Hazeleger, P. de Vries, and M. Cane. 2005. Pathways into the Pacific Equatorial Undercurrent: A trajectory analysis. *Journal of Physical Oceanography* 35:2,134–2,151, <https://doi.org/10.1175/JPO2825.1>.
- Grenier, M., S. Cravatte, B. Blanke, C. Menkes, A. Koch-Larrouy, F. Durand, A. Melet, and C. Jeandel. 2011. From the western boundary currents to the Pacific equatorial undercurrent: Modeled pathways and water mass evolutions. *Journal of Geophysical Research* 116, C12044, <https://doi.org/10.1029/2011JC007477>.
- Hazeleger, W., M. Visbeck, M. Cane, A. Karspeck, and M. Naik. 2001. Decadal upper ocean temperature variability in the tropical Pacific. *Journal of Geophysical Research* 106:8,971–8,988, <https://doi.org/10.1029/2000JC000536>.
- Henry, D. 2013. An exact solution for equatorial geophysical water waves with an underlying current. *European Journal of Mechanics - B/Fluids* 38:18–21, <https://doi.org/10.1016/j.euromechflu.2012.10.001>.
- Henry, D. 2016. Equatorially trapped nonlinear water waves in a  $\beta$ -plane approximation with centripetal forces. *Journal of Fluid Mechanics* 804, R1, <https://doi.org/10.1017/jfm.2016.544>.
- Johnson, G.C., M.J. McPhaden, and E. Firing. 2001. Equatorial Pacific Ocean horizontal velocity, divergence, and upwelling. *Journal of Physical Oceanography* 31(3):839–849, [https://doi.org/10.1175/1520-0485\(2001\)031<0839:EPOHVD>2.0.CO;2](https://doi.org/10.1175/1520-0485(2001)031<0839:EPOHVD>2.0.CO;2).
- Karnauskas, K.B., and A.L. Cohen. 2012. Equatorial refuge amid tropical warming. *Nature Climate Change* 2(7):530–534, <https://doi.org/10.1038/nclimate1499>.
- Knauss, J.A., and J.E. King. 1958. Observations of the Pacific Equatorial Undercurrent. *Nature* 158:601–602, <https://doi.org/10.1038/182601a0>.
- Lu, P., J.P. McCreary, and B.A. Klinger. 1998. Meridional circulation cells and the source waters of the Pacific Equatorial Undercurrent. *Journal of Physical Oceanography* 28:62–84, [https://doi.org/10.1175/1520-0485\(1998\)028<0062:MCCATS>2.0.CO;2](https://doi.org/10.1175/1520-0485(1998)028<0062:MCCATS>2.0.CO;2).
- Lukas, R. 1986. The termination of the equatorial undercurrent in the Eastern Pacific. *Progress in Oceanography* 16:63–90, [https://doi.org/10.1016/0079-6611\(86\)90007-8](https://doi.org/10.1016/0079-6611(86)90007-8).
- McCreary, J.P. 1981. A linear stratified ocean model of the equatorial undercurrent. *Philosophical Transactions of the Royal Society A* 298:603–635, <https://doi.org/10.1098/rsta.1981.0002>.
- McCreary, J.P. Jr. 1985. Modeling equatorial ocean circulation. *Annual Review of Fluid Mechanics* 17(1):359–409, <https://doi.org/10.1146/annurev.fl.17.010185.002043>.
- McCreary, J.P. Jr., and P. Lu. 1994. Interaction between the subtropical and equatorial ocean circulations: The subtropical cell. *Journal of Physical Oceanography* 24:466–497.
- McKee, W.D. 1973. The wind-driven equatorial circulation in a homogeneous ocean. *Deep Sea Research and Oceanographic Abstracts* 20:889–899, [https://doi.org/10.1016/0011-7471\(73\)90107-1](https://doi.org/10.1016/0011-7471(73)90107-1).
- Pedlosky, J. 1987. Thermocline theories. Pp. 55–101 in *General Circulation of the Ocean*. Springer.
- Qin, X., A. Sen Gupta, and E. van Sebille. 2015. Variability in the origins and pathways of Pacific Equatorial Undercurrent water. *Journal of Geophysical Research* 120:3,113–3,128, <https://doi.org/10.1002/2014JC010549>.

- Rayn, J.P., I. Ueki, Y. Chao, H. Zhang, P.S. Polito, and F.P. Chavez. 2006. Western Pacific modulation of large phytoplankton blooms in the central and eastern equatorial Pacific. *Journal of Geophysical Research* 111, G02013, <https://doi.org/10.1029/2005JG000084>.
- Robinson, A.R. 1966. An investigation into the wind as the cause of the equatorial undercurrent. *Journal of Marine Research* 24:179–204.
- Schneider, N., S. Venzke, A.J. Miller, D.W. Pierce, T.P. Barnett, C. Deser, and M. Latif. 1999. Pacific thermocline bridge revisited. *Geophysical Research Letters* 26:1,329–1,332, <https://doi.org/10.1029/1999GL900222>.
- Stommel, H. 1960. Wind-drift near the equator. *Deep Sea Research* 6:298–302, [https://doi.org/10.1016/0146-6313\(59\)90088-7](https://doi.org/10.1016/0146-6313(59)90088-7).
- Talley, L.D., G.L. Pickard, W.J. Emery, and J.H. Swift. 2011. *Descriptive Physical Oceanography: An Introduction*. Academic Press, 560 pp.
- Tsuchiya, M., R. Lukas, and F.A. Fine. 1989. Source waters of the Pacific equatorial undercurrent. *Progress in Oceanography* 23:101–147, [https://doi.org/10.1016/0079-6611\(89\)90012-8](https://doi.org/10.1016/0079-6611(89)90012-8).
- Vallis, G.K. 2006. *Atmospheric and Oceanic Fluid Dynamics*. Cambridge University Press.
- Veronis, G. 1960. An approximate theoretical analysis of the equatorial undercurrent. *Deep Sea Research* 6:318–327, [https://doi.org/10.1016/0146-6313\(59\)90091-7](https://doi.org/10.1016/0146-6313(59)90091-7).
- Wyrki, K., and B. Kilonsky. 1984. Mean water and current structure during the Hawaii-to-Tahiti shuttle experiment. *Journal of Physical Oceanography* 14:242–254, [https://doi.org/10.1175/1520-0485\(1984\)014<0242:MWACSD>2.0.CO;2](https://doi.org/10.1175/1520-0485(1984)014<0242:MWACSD>2.0.CO;2).
- Zhang, R.-H., L.M. Rothstein, and A.J. Busalacchi. 1998. Origin of upper-ocean warming and El Niño change on decadal time scales in the tropical Pacific Ocean. *Nature* 391:879–883, <https://doi.org/10.1038/36081>.

## ACKNOWLEDGMENTS

Discussions with Robin Stanley Johnson, Newcastle upon Tyne University, UK, and suggestions given by him are gratefully acknowledged. Helpful suggestions from the reviewers are also appreciated.

## AUTHOR

**Biswajit Basu** (basub@tcd.ie) is Professor, Trinity College Dublin, Ireland.

## ARTICLE CITATION

Basu, B. 2018. On a three-dimensional nonlinear model of Pacific equatorial ocean dynamics: Velocities and flow paths. *Oceanography* 31(3):51–58, <https://doi.org/10.5670/oceanog.2018.309>.